Journal of King Saud University – Science 32 (2020) 1937–1943

Contents lists available at ScienceDirect

Journal of King Saud University – Science

journal homepage: www.sciencedirect.com

Original article

Metal organic precursor derived $Ba_{1-x}Ca_xZrO_3$ ($0.05 \leq x \leq 0.20$) nanoceramics for excellent capacitor applications

Mohd Ubaidullah [a,b,*], Jahangeer Ahmed [a], Abdullah M. Al-Enizi [a], Akshi Tyagi [c], Shoyebmohamed F. Shaikh [a], Nazia Tarannum [d], Tokeer Ahmad [b,*]

[a] Department of Chemistry, College of Science, King Saud University, Riyadh 11451, Saudi Arabia
[b] Nanochemistry Lab, Department of Chemistry, Jamia Millia Islamia, New Delhi 110025, India
[c] Department of Chemistry, Indian Institute of Technology Kanpur, Kanpur, Uttar Pradesh 208016, India
[d] Department of Chemistry, Chaudhary Charan Singh University, Meerut 250005, Uttar Pradesh, India

ARTICLE INFO

Article history:
Received 14 December 2019
Revised 5 February 2020
Accepted 5 February 2020
Available online 13 February 2020

Keywords:
Synthesis
Nanoceramics
Surface area
Energy storage and conversion

ABSTRACT

Monophasic nanoceramics of calcium doped barium zirconate (BCZ) $Ba_{1-x}Ca_xZrO_3$ (x = 0.0, 0.05, 0.10, 0.15 and 0.20) have been manufactured *via* easy and cost effective metal organic precursor route at 1000 °C. The structural elucidations of the BCZ nanoparticles were confirmed by different analytical techniques i.e. SEM, TEM, XRD etc. Moreover, the elemental composition and detailed surface area were estimated through EDS/EDX and BET analysis. TEM particle sizes of $Ba_{1-x}Ca_xZrO_3$ (x = 0.0, 0.05, 0.10, 0.15 and 0.20) were found in the range of 75–42 nm. Mixed (spherical, hexagonal and cubic) morphology and shapes of the nanoceramics were established by SEM and TEM studies. The incorporation of calcium to $BaZrO_3$ host lattice confirmed by EDS/EDX studies. Very high specific surface area was achieved (233–271 $m^2\ g^{-1}$) for $Ba_{1-x}Ca_xZrO_3$ (x = 0.0, 0.05, 0.10, 0.15 and 0.20) nanoceramics which is corroborated well with TEM particle size and pore (BJH and DA) size studies. Excellent dielectric properties of BCZ were found at room temperature in the frequency range of 20 kHz to 1 MHz. As the concentration of Ca^{2+} ion increased the values of dielectric constant were found to increase (48.1–284.7). High surface area and excellent porosity with high dielectric constant of BCZ could make it as an ideal material for energy devices.

1. Introduction

The drastic climate change and deteriorating environment is due to the superfluous use of fossil fuel use instead is the prime concern globally. The quest of low cost and extremely efficient energy materials is the moon shot for scientific community. Perovskite materials played a very important role in different kinds of applications. ABO_3 type of perovskite; which can accommodate a group of materials widely used in different applications i.e. optical (Erb et al., 1997) magnetic (Zhang et al., 2014) electric (Ahmad et al., 2017) and catalytic properties (Athawale et al., 2006) as well as in wireless communication (Beckers et al., 1996; Gonenli and Tas, 1999; Mathews et al., 1997; Yugami et al., 1995; Zhao et al., 1996) Moreover; the functional behavior such as superconductivity, ferro electricity and photo electrochemical sensitivity (Al-Hartomy et al., 2012) also shown by perovskite materials.

In past, zirconates of metals (M = Ca, Pb, Sr and Ba) explored for potential applications in heterogeneous catalysis (Nair et al., 1998) electrical ceramics (Osaka et al., 1999) and refractories. Barium zirconate/titanate has gained considerable attention due to having diverse functionality in solid oxide fuel cell (Bohn and Schober, 2000; Kreuer, 2003; Yamazaki et al., 2009) photoluminescence (Cavalcante et al., 2009) photocatalysis(Wang et al., 2006)dielectrics (Al-Hartomy et al., 2013) microwave resonators (Yamaguchi et al., 1980) and high temperature superconductors (Erb et al., 1995) At 27 °C, $BaZrO_3$ show an ideal cubic (Pm3m) perovskite structure (Megaw, 1946) Owing to high melting point (2700 °C) and small thermal expansion coefficient ($0.87x10^{-5}$°C between 25 and 1080 °C) It is frequently used as commercial

* Corresponding authors at: Department of Chemistry, College of Science, King Saud University, Riyadh 11451, Saudi Arabia (M. Ubaidullah).
E-mail addresses: mtayyab@ksu.edu.sa (M. Ubaidullah), tahmad3@jmi.ac.in (T. Ahmad).

Peer review under responsibility of King Saud University.

Production and hosting by Elsevier

https://doi.org/10.1016/j.jksus.2020.02.009
1018-3647/

dielectric materials. Moreover, various metal ions doped $BaZrO_3$ found suitable for optical (Borja-Urby et al., 2011) electrical (Parida et al., 2012) catalytic (Yuan et al., 2010) and sensing (Iwahara et al., 1993) applications. Numerous preparation methods used for the preparation of nanostructured materials. These procedures entail both chemical and physical routes such as reverse micelle (Ranjan et al., 2009) co-precipitation (Gandhi et al., 2014) solvothermal (AHMAD et al., 2013) sonochemical (Nag et al., 2012) sol-gel synthesis(Pfaff, 1994) hydrothermal (Ganguly et al., 2010) chemical vapor deposition (CVD) (Bhaviripudi et al., 2007) evaporation-condensation method (Choi et al., 2002) gas phase reaction (Zak et al., 2000) plasma synthesis (Irzh et al., 2010) and polymeric citrate precursor method (Ahmad et al., 2015).

Herein, cost effective and alkoxides free preparation of $Ba_{1-x}Ca_xZrO_3$ ($0.0 \leq x \leq 0.20$) with different Ca^{+2} concentrations presented via metal organic procedure for the first time. The as prepared nanoceramics were characterized by different analytical techniques for their possible use in energy applications.

2. Experimental

In the synthesis of BCZ nanoceramics; Barium acetate (Qualigens; 99.5%), calcium acetate (Alfa Aesar, 99%), citric acid (Spectrochem; 99%), zirconium oxychloride (CDH; 99%) and ethylene glycol (SD fine-chem Ltd.) were used without any purification. 0.1 M aqueous solutions of barium acetate, calcium acetate and zirconium oxychloride were made using DDW water. In a beaker ethylene glycol (1.4 mL) was added. Under constant stirring, 25 mL of 0.1 M zirconium oxychloride was added to this to get a clear and transparent solution followed by adding of dry citric acid (0.11 mol). After addition of citric acid slight turbidity was seen after 3.5 h stirring at room temperature the solution become clear. Aqueous solutions of 0.1 M barium and calcium acetate were added with controlled stoichiometry. The nucleation was started by the addition of the metal acetates at room temperature (25 °C). Thereafter, to obtain a homogeneous and viscous reaction mixture of metal ions followed by the stirring at 55 ± 5 for 2 h. The resulting mixture was treated at 135 ± 5 for 20 h to promote the poly-condensation reaction. A viscous resin (i.e. polymeric gel) was obtained, and then fired in muffle furnace at 300°Cfor 2 h. The black colored powder sample was formed, which is used as the precursor materials in the synthesis of BCZ nanoparticles. A creamy white powder of $Ba_{1-x}Ca_xZrO_3$ (BCZ) was obtained by the firing of the precursor at 1000 °C. A flow chart containing synthetic steps for the synthesis of BCZ nanoparticles was given as in Scheme 1.

Numerous analytical techniques were used for the characterization of as prepared ceramic materials ($Ba_{1-x}Ca_xZrO_3$). The crystalline nature of $Ba_{1-x}Ca_xZrO_3$ was characterized powder x-ray diffractometer (Bruker, D8). High resolution-TEM (HR-TEM) analysis was performed on (FEI Technai G^2 20) electron microscope at 200 kVA to examine shape and size of nanoceramics. For sample preparation, a pinch of the powder added in ethanol followed by sonication. Small drop of the dispersed solution was kept on the porous copper grid coated with carbon. FE-SEM (JEOL, JSM-7600F), was performed at 5kVto check the surface texture and morphology of nanoceramics. Energy dispersive x-ray studies (EDAX) were employed for the elemental analysis with 127 eV Bruker EDX detector. Note that EDAX was equipped with SEM machine.

Nitrogen adsorption desorption (N_2 A-D) analysis was performed on Quantachrome instrument 2000e to get the detailed surface area and porosity. The adsorbed contaminates and gases onto the sample were removed by the degassing process at 250 °C for 3 h. The specific surface areas of nanoceramics were estimated using multipoint BET equation. The porosity of the samples

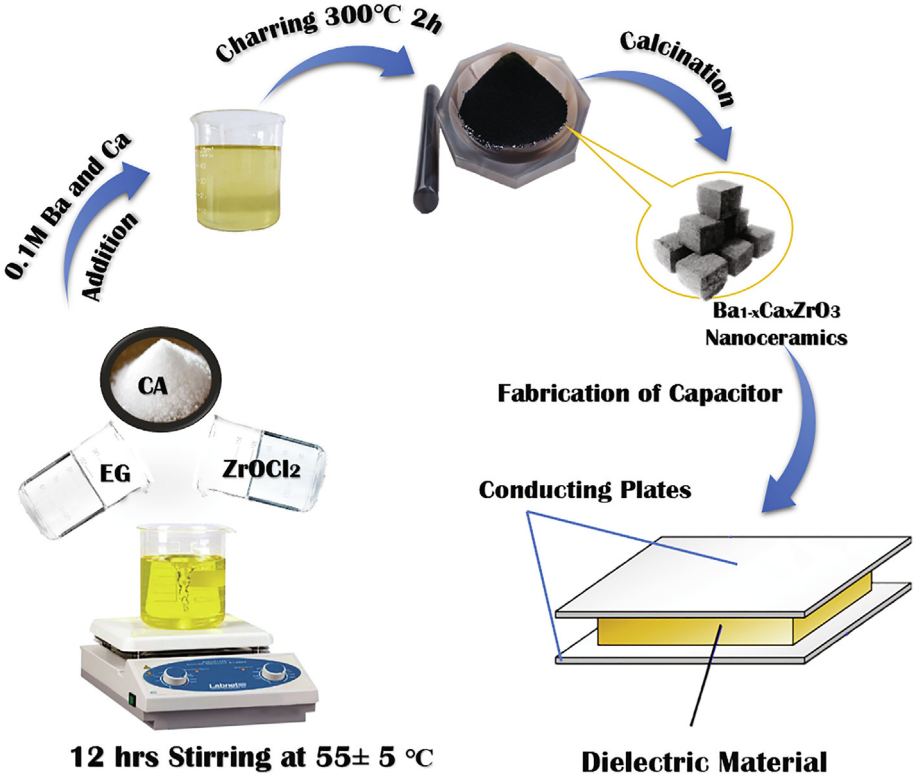

Scheme 1. Schematic representation of synthesis procedure of $Ba_{1-x}Ca_xZrO_3$ ($0 \leq x \leq 0.20$) nanoparticles using metal organic precursor method.

was also investigated with the help of BJH (Barrett–Joyner–Halen da) and DA (Dubinin-Astakhov) models which is correlated to mesoporous and microporous adsorption phenomenon.

The dielectric behaviors of the nanoceramics have been investigated on sintered pellets by using high frequency LCR meter (Wayne Kerr, 6505P, UK) at a range of 20 kHz to 1 MHz. Both the faces of pellets were coated by silver paste and dried at 90 °C for 1 h. Thickness and diameter of the pellet were noted in order to quantify the accurate value of dielectric constant and loss. The open and closed circuit calibration were performed to decrease the parasitic effect arising from the LCR equipment.

3. Results and discussion

3.1. Structural interpretation

3.1.1. Electron microscopic studies

Surface architecture and morphology were inspected by FE-SEM while shape and size of the nanoceramics $Ba_{1-x}Ca_xZrO_3$ (0–0.20) were estimated through HR-TEM. The SEM micrographs are shown in Fig. 1(a-e). Irregular shape of the particles observed in SEM micrographs. As the Ca^{2+} content increases, the aggregation of the particle in the solid solution increases. Fig. 1a depicts the least agglomeration of the particles of pure $BaZrO_3$.

Fig. 2 depicts the TEM images of $Ba_{1-x}Ca_xZrO_3$ (x = 0.0, 0.05, 0.10, 0.15 and 0.20). It is evident from the TEM images that particles are in irregular shapes (cubic, spherical, and hexagonal) with slight agglomeration on heat treatment at 1000 °C in air. The average particle size was valued to 42–75 nm. As the concentration of dopant increases from 0 to 0.20, the particle size decreases from 75 to 42 nm. Fig. 2a shows the TEM micrographs of $BaZrO_3$ nanoparticles (~75 nm). However the smallest particle size of 42 nm is shown by $Ba_{0.95}Ca_{0.20}ZrO_3$ nanoparticles. The observed agglomeration is due to the fusion or overlapping of grains. The big size of the particles tends to the aggregation of smaller articles. TEM particle size support well with specific surface area, smaller particle size showed high surface area.

The chemical composition of calcium doped barium zirconate solid solution was calculated from the EDS/EDX studies as shown in Fig. 3. No extra element was appeared in pure $BaZrO_3$ except O, Zr and Ba (Fig. 3a). For the initial calcium composition (5%), a peak of calcium was observed in spectra, which shows the incorporation of Ca^{2+} in $BaZrO_3$ matrix. It is apparent from the micrographs (Fig. 3(b-e)) as the calcium content increases, the intensity of calcium peaks also increases. The loaded compositions of Ca^{2+} were found to have a very close agreement with the experimentally calculated compositions of solid solution.

3.1.2. Powder X-ray diffraction studies (P-XRD)

Phase purity and crystal structure system of $Ba_{1-x}Ca_xZrO_3$ ($0 \leq x \leq 0.20$) nanoceramics were confirmed P-XRD studies as shown in Fig. 4 All reflections appeared in diffraction patterns satisfactorily indexed with monophasic cubic system of $BaZrO_3$ (JCPDS No. 74-1299). The doping of Ca^{2+} at Ba^{2+} lattice site confirmed by the monotonic shift of the reflections towards higher angle of diffraction patterns. No other phase was detected in XRD, which reveals the formation of pure phase of $BaZrO_3$ solid solution. $BaZrO_3$ lattice marginally contracts owing to the incorporation of Ca^{2+} into $BaZrO_3$ lattice site as also expected because of the smaller ionic radius of Ca^{2+} (1.00 Å) compared to Ba^{2+} (1.35 Å) (Shannon, 1976).

3.2. Surface area and porosity analysis

N2 adsorption desorption isotherm was recorded by Brunauer-Emmett-Teller (BET) gas adsorption technique to analyze the

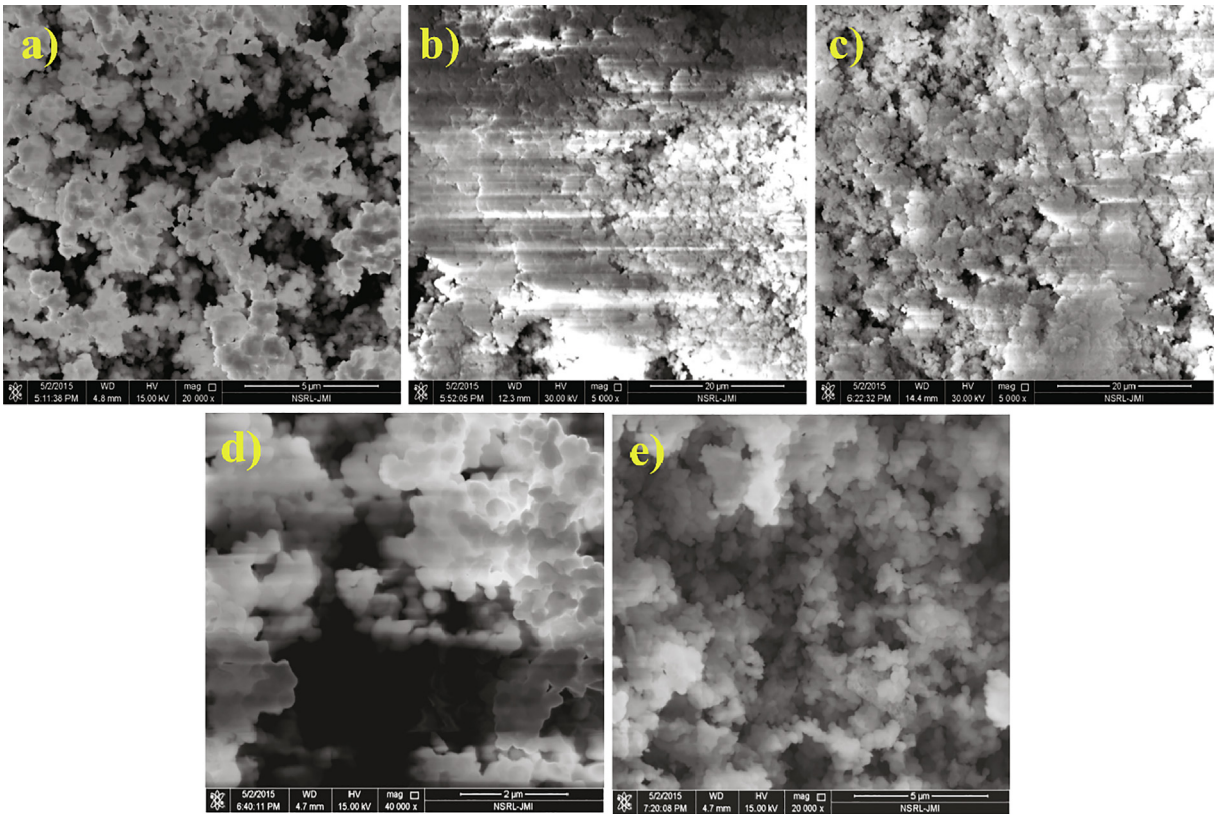

Fig. 1. SEM micrographs of $Ba_{1-x}Ca_xZrO_3$ nanoparticles for (a) x = 0, (b) x = 0.05, (c) x = 0.10, (d) x = 0.15 and (e) x = 0.20.

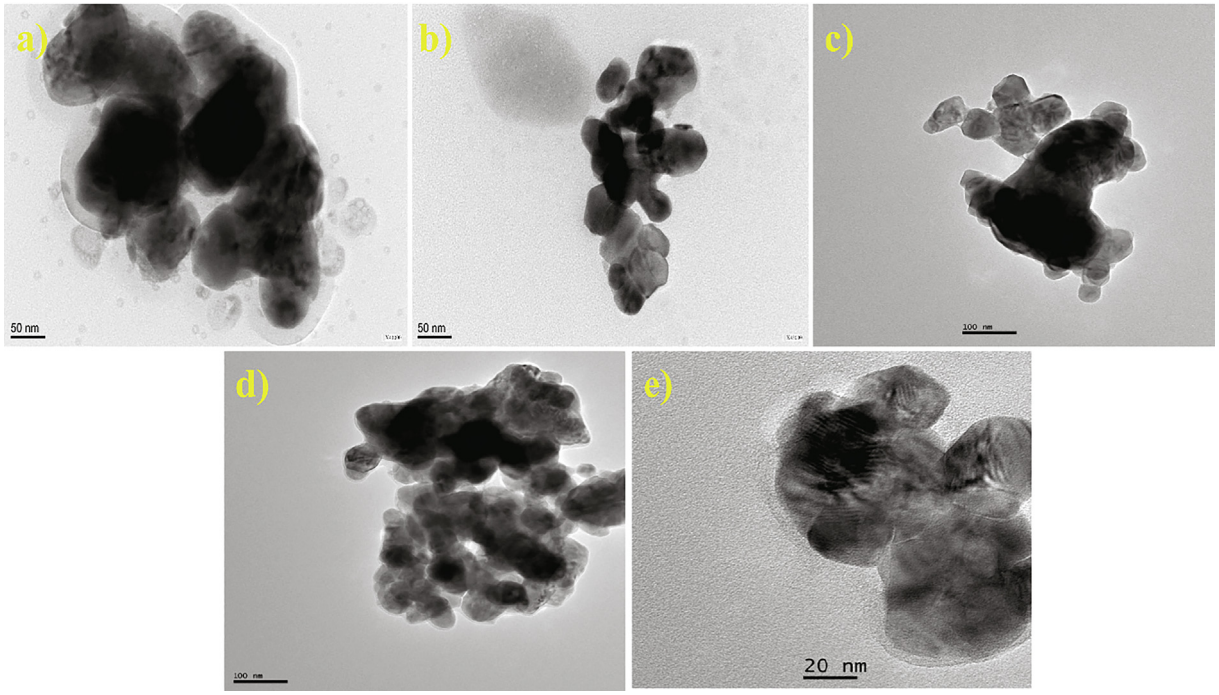

Fig. 2. TEM micrographs of $Ba_{1-x}Ca_xZrO_3$ nanoparticles for (a) x = 0, (b) x = 0.05, (c) x = 0.10, (d) x = 0.15 and (e) x = 0.20.

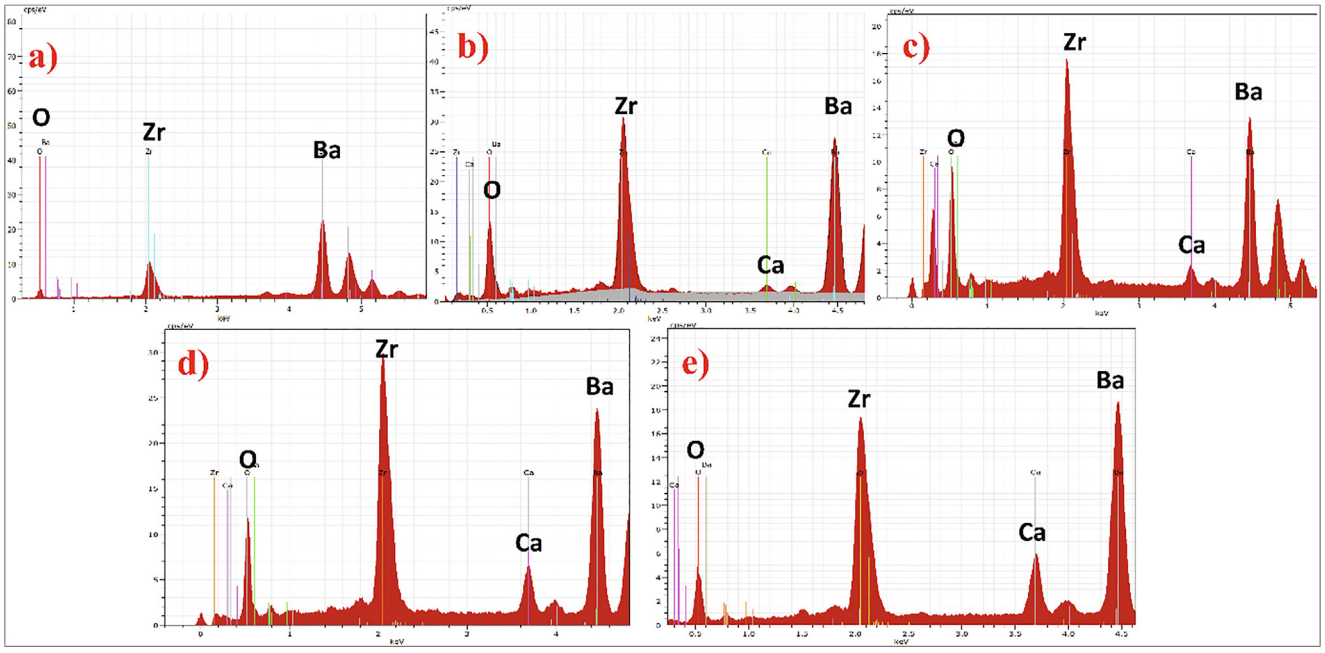

Fig. 3. EDS/EDX micrographs of $Ba_{1-x}Ca_xZrO_3$ nanoceramics for (a) x = 0, (b) x = 0.05, (c) x = 0.10, (d) x = 0.15 and (e) x = 0.20.

surface area and porosity of nanoceramics Fig. 5(a-d). A range of 233–271 m^2/g specific surface area was achieved for $Ba_{1-x}Ca_xZrO_3$ ($0 \leq x \leq 0.20$). Note that the surface area was found to increase from 233–271 m^2/g as the Ca content increases in the solid solution which is due to the decrease in particle size. Fig. 5a illustrate the type III adsorption desorption isotherm which clearly indicate the multilayer adsorption of the N2. Pore size distribution studies of $Ba_{1-x}Ca_xZrO_3$ ($0 \leq x \leq 0.20$) nanoceramics have been carried out using the BJH (Barrett–Joyner–Halenda) and DA (Dubinin–Astakhov) methods. Fig. 5c shows the DA pore radius of the nanoceramics. The pore radius of these nanoparticles was found to be in the range from16.24 to 16.40 Å and14.80 to 15.00 Å using BJH model and DA method respectively. The values of pore radius by using BJH and DA models were found to be nearly similar with slight variation. Fig. 5d shows the change in surface area and porosity on changing the composition of the materials. It is evident from Fig. 5d that as the value of specific surface area increases, BJH pore radius decreases accordingly with composition. The highest surface area (271 m^2/g) has the lowest BJH pore radius (16.24 Å) and vice versa, as shown in Table 1 and Fig. 5d.

Table 1 illustrates the detailed surface area and porosity (BJH and DA) distributions of $Ba_{1-x}Ca_xZrO_3$ ($0 \leq x \leq 0.20$) nanoceramics.

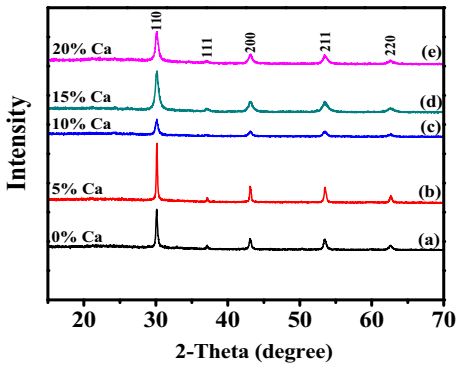

Fig. 4. X-ray diffraction of $Ba_{1-x}Ca_xZrO_3$ nanoparticles for (a) x = 0, (b) x = 0.05, (c) x = 0.10, (d) x = 0.15 and (e) x = 0.20.

The BJH and DA pore size studies corroborate perfectly with surface area values, as the value of surface area increase the decrease in BJH and DA pore radius observed.

3.3. Dielectric properties

Dielectric behaviors of the nanoceramics ($Ba_{1-x}Ca_xZrO_3$ ($0 \leq x \leq 0.20$)) were at 20 kHz to 1 MHz range at 27 °C. Fig. 6(a-e) demonstrate the variation in dielectric behaviour as a function of frequency for all compositions. At low frequency region, slight drop in dielectric constant and at higher frequencies the dielectric constant was found to be stable for all the compositions which is associated to the Maxwell–Wagner interfacial principle (Prodromakis and Papavassiliou, 2009). However slight increase in dielectric loss was found on increasing the frequency. Table 2 comprises the values of dielectric constant and dielectric loss with composition at 100 kHz. The highest value (284.7) of dielectric constant was found for $Ba_{0.80}Ca_{0.20}ZrO_3$ having the highest surface area (271 m^2/g) while the lowest value of dielectric constant (48.1) was found for $BaZrO_3$ having lowest surface area (233 m^2/g). The increase in the dielectric constant related to the increase in the specific surface area of nanoceramics due to which the number of electric dipoles increases on the surface and contributes to the polarizability of material.

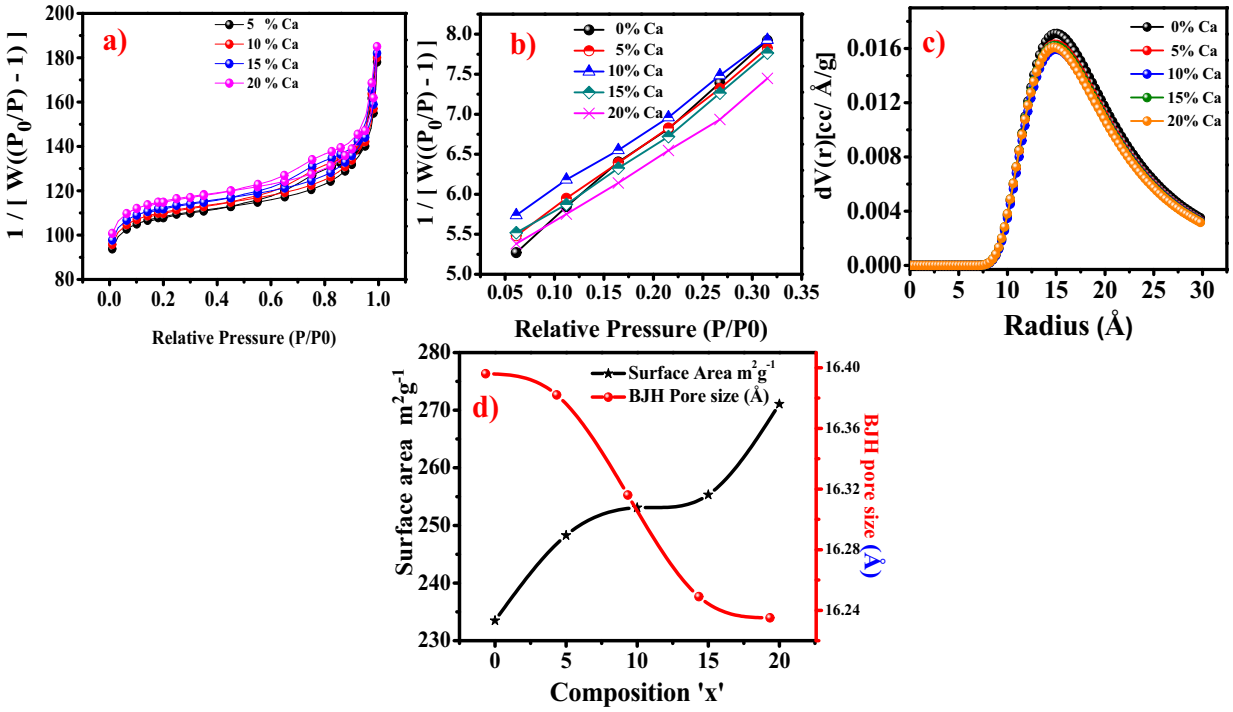

Fig. 5. (a) N2 A-D isotherm of Ca 5% (b) multipoint BET overlay (c) DA pore size distribution overlay (d) variation in surface area and BJH pore size with composition of $Ba_{1-x}Ca_xZrO_3$ ($0 \leq x \leq 0.20$) nanoceramics.

Table 1
BET surface area, TEM size, BJH and DA pore sizes of $Ba_{1-x}Ca_xZrO_3$ ($0 \leq x \leq 0.20$) nanoceramics.

S. No.	Composition	Surface Area (m^2g^{-1})	TEM Particle Size (nm)	BJH Pore Size (Å)	DA Pore Size (Å)
1	$BaZrO_3$	233	75	16.40	15.00
2	$Ba_{0.95}Ca_{0.05}ZrO_3$	248	62	16.38	14.95
3	$Ba_{0.90}Ca_{0.10}ZrO_3$	253	55	16.32	14.90
4	$Ba_{0.85}Ca_{0.15}ZrO_3$	255	51	16.25	14.85
5	$Ba_{0.80}Ca_{0.20}ZrO_3$	271	42	16.24	14.80

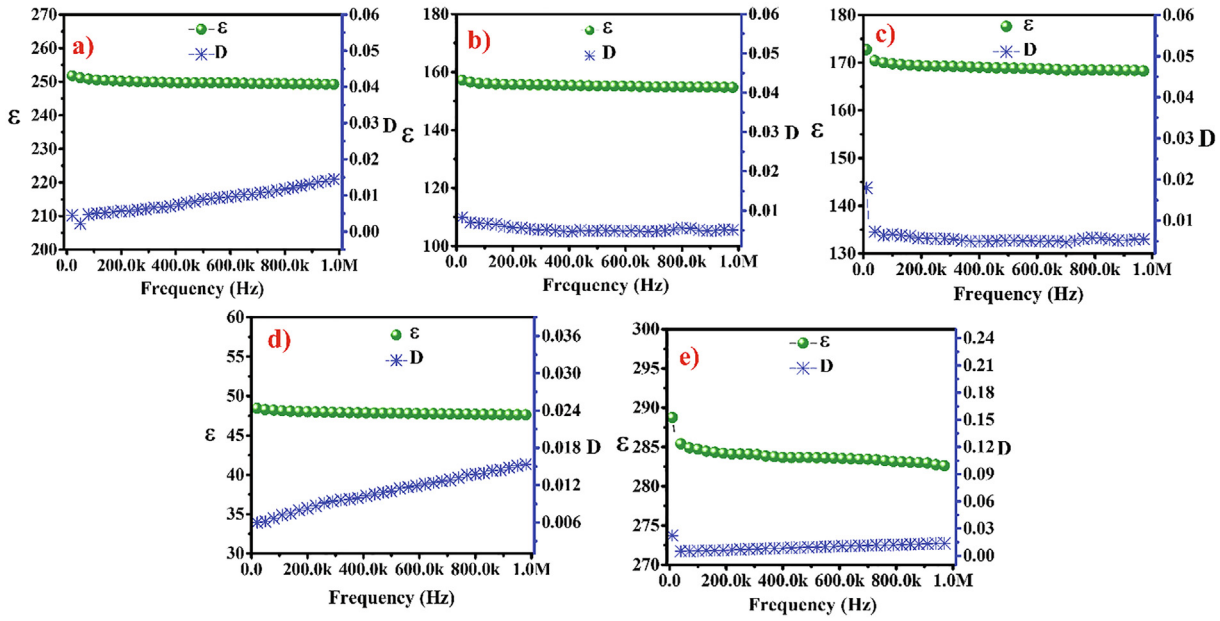

Fig. 6. Change in dielectric constant and dielectric loss of $Ba_{1-x}Ca_xZrO_3$for (a) x = 0, (b) x = 0.05, (c) x = 0.10, (d) x = 0.15 and I x = 0.20 nanoparticles with frequency at room temperature.

Table 2
Room temperature dielectric constant and loss of Ba1-xCaxZrO3 ($0 \leq x \leq 0.20$) nanoparticles at 100 kHz.

S. No.	Composition	Dielectric Constant	Dielectric Loss
1.	$BaZrO_3$	48.13	0.007
2.	$Ba_{0.95}Ca_{0.05}ZrO_3$	156.05	0.006
3.	$Ba_{0.90}$ $Ca_{0.10}ZrO_3$	169.78	0.006
4.	$Ba_{0.85}$ $Ca_{0.15}ZrO_3$	250.60	0.005
5.	$Ba_{0.80}$ $Ca_{0.20}ZrO_3$	284.71	0.005

4. Conclusions

Monophasic nanoceramics of $Ba_{1-x}Ca_xZrO_3$ (x = 0.0, 0.05, 0.10, 0.15 and 0.20) have been prepared by simple and cost effective metal organic precursor route for the first time. X-ray diffraction patterns confirmed the highly crystalline nature of the nanoparticles. The particles sizes estimated by TEM were found75-42 nm. Slight agglomeration could be seen in SEM micrographs. The surface area corroborated well with the TEM particles size as surface area increases from 233-271 m^2/g TEM particles size decreasing 75–42 nm. The specific surface increased on increasing the dopant (Ca^{2+}) concentration, while pore size decrease (BJH and DA). The highest value of dielectric constant (284.7) and small value of dielectric loss (0.005) at 100 kHz was found for 20% Ca-doped $BaZrO_3$ which has highest surface area (271 m^2g^{-1}) and smallest particle size of 42 nm. The dielectric loss is found to be very small for all the compositions showing that the material is worthy for high frequency device applications. High surface area and excellent porosity with high dielectric constant of BCZ could make it as an ideal material for energy devices.

Declaration of Competing Interest

The authors declare that they have no known competing financial interests or personal relationships that could have appeared to influence the work reported in this paper.

Acknowledgement

The authors extend their sincere appreciation to researchers supporting project number (RSP-2019/55), King Saud University, Riyadh, Saudi Arabia for funding this research.

References

Ahmad, T., Khatoon, S., Coolahan, K., 2013. Optical, magnetic and structural characterization of Zn1 − xCoxO nanoparticles synthesized by solvothermal method. Bull. Mater. Sci. 36, 997–1004. https://doi.org/10.1007/s12034-013-0569-6.

Ahmad, T., Lone, I.H., Ubaidullah, M., 2015. Structural characterization and multiferroic properties of hexagonal nano-sized YMnO3 developed by a low temperature precursor route. RSC Adv. 5, 58065–58071. https://doi.org/10.1039/C5RA09038E.

Ahmad, T., Ubaidullah, M., Lone, I.H., Kumar, D., Al-Hartomy, O.A., 2017. Microemulsion synthesis, structural characterization and dielectric properties of Ba1-xPbxZrO3 ($0.05 \leq x \leq 0.20$) nanoparticles. Mater. Res. Bull. 89, 185–192. https://doi.org/10.1016/j.materresbull.2017.01.044.

Al-Hartomy, O.A., Ubaidullah, M., Khatoon, S., Madani, J.H., Ahmad, T., 2012. Synthesis, characterization, and dielectric properties of nanocrystalline Ba1−xPbxZrO3 ($0 \leq x \leq 0.75$) by polymeric citrate precursor route. J. Mater. Res. 27, 2479–2488. https://doi.org/10.1557/jmr.2012.242.

Al-Hartomy, O.A., Ubaidullah, M., Kumar, D., Madani, J.H., Ahmad, T., 2013. Dielectric properties of Ba1-xSrxZrO3 ($0 \leq x \leq 1$) nanoceramics developed by citrate precursor route. J. Mater. Res. 28, 1070–1077. https://doi.org/10.1557/jmr.2013.40.

Athawale, A.A., Chandwadkar, A.J., Karandikar, P., Pasricha, R., Bapat, M.S., 2006. Radiation assisted synthesis of nanosized barium zirconate. Radiat. Phys. Chem. 75, 755–759. https://doi.org/10.1016/j.radphyschem.2005.12.041.

Beckers, L., Sanchez, F., Schubert, J., Zander, W., Buchal, C., 1996. Epitaxial growth of Y-doped SrZrO3 films on MgO by pulsed laser deposition. J. Appl. Phys. 79, 3337–3339. https://doi.org/10.1063/1.361234.

Bhaviripudi, S., Mile, E., Steiner, S.A., Zare, A.T., Dresselhaus, M.S., Belcher, A.M., Kong, J., 2007. CVD synthesis of single-walled carbon nanotubes from gold nanoparticle catalysts. J. Am. Chem. Soc. 129, 1516–1517. https://doi.org/10.1021/ja0673332.

Bohn, H.G., Schober, T., 2000. Electrical conductivity of the high-temperature proton conductor BaZr0.9Y0.1O2.95. J. Am. Ceram. Soc. 83, 768–772. https://doi.org/10.1111/j.1151-2916.2000.tb01272.x.

Borja-Urby, R., Díaz-Torres, L.A., Salas, P., Moctezuma, E., Vega, M., Ángeles-Chávez, C., 2011. Structural study, photoluminescence, and photocatalytic activity of semiconducting BaZrO3: Bi nanocrystals. Mater. Sci. Eng., B 176, 1382–1387. https://doi.org/10.1016/j.mseb.2011.01.024.

Cavalcante, L.S., Sczancoski, J.C., Espinosa, J.W.M., Mastelaro, V.R., Michalowicz, A., Pizani, P.S., Vicente, F.S. De, Li, M.S., Varela, J.A., Longo, E., 2009. Intense blue and

green photoluminescence emissions at room temperature in barium zirconate powders. J. Alloy. Compd. 471, 253–258. https://doi.org/10.1016/j.jallcom.2008.03.080.

Choi, C.J., Tolochko, O., Kim, B.K., 2002. Preparation of iron nanoparticles by chemical vapor condensation. Mater. Lett. 56, 289–294. https://doi.org/10.1016/S0167-577X(02)00457-3.

Erb, A., Walker, E., Flükiger, R., 1995. BaZrO3: the solution for the crucible corrosion problem during the single crystal growth of high-Tc superconductors REBa2Cu3O7−δ; RE = Y, Pr. Physica C 245, 245–251. https://doi.org/10.1016/0921-4534(95)00123-9.

Erb, A., Walker, E., Genoud, J.-Y., Flükiger, R., 1997. 10 years of crystal growth of the 123- and 124- high Tc superconductors: from Al2O3 to BaZrO3 progress in crystal growth and sample quality and its impact on physics. Physica C 282–287, 459–460. https://doi.org/10.1016/S0921-4534(97)00312-2.

Gandhi, V., Ganesan, R., Abdulrahman Syedahamed, H.H., Thaiyan, M., 2014. Effect of cobalt doping on structural, optical, and magnetic properties of ZnO nanoparticles synthesized by coprecipitation method. J. Phys. Chem. C 118, 9715–9725. https://doi.org/10.1021/jp411848t.

Ganguly, A., Ahmad, T., Ganguli, A.K., 2010. Silica mesostructures: control of pore size and surface area using a surfactant-templated hydrothermal process. Langmuir 26, 14901–14908. https://doi.org/10.1021/la102510c.

Gonenli, I.E., Tas, A.C., 1999. Chemical synthesis of pure and Gd-doped CaZrO3 powders. J. Eur. Ceram. Soc. 19, 2563–2567. https://doi.org/10.1016/S0955-2219(99)00130-2.

Irzh, A., Genish, I., Klein, L., Solovyov, L.A., Gedanken, A., 2010. Synthesis of ZnO and Zn nanoparticles in microwave plasma and their deposition on glass slides. Langmuir 26, 5976–5984. https://doi.org/10.1021/la904499s.

Iwahara, H., Yajima, T., Hibino, T., Ozaki, K., Suzuki, H., 1993. Protonic conduction in calcium, strontium and barium zirconates. Solid State Ionics 61, 65–69. https://doi.org/10.1016/0167-2738(93)90335-Z.

Kreuer, K.D., 2003. Proton-conducting oxides. Annu. Rev. Mater. Res. 33, 333–359. https://doi.org/10.1146/annurev.matsci.33.022802.091825.

Mathews, S., Ramesh, R., Venkatesan, T., Benedetto, J., 1997. Ferroelectric field effect transistor based on epitaxial perovskite heterostructures. Science 276, 238–240. https://doi.org/10.1126/science.276.5310.238.

Megaw, H.D., 1946. Crystal structure of double oxides of the perovskite type. Proceedings of the Physical Society 58, 133–152. doi: 10.1088/0959-5309/58/2/301.

Nag, P., Banerjee, S., Lee, Yongmoon, Bumajdad, A., Lee, Yongjae, Devi, P.S., 2012. Sonochemical synthesis and properties of nanoparticles of FeSbO4. Inorg. Chem. 51, 844–850. https://doi.org/10.1021/ic201353u.

Nair, J., Nair, P., Doesburg, E.B.M., van Ommen, J.G., Ross, J.R.H., Burggraaf, A.J., Mizukami, F., 1998. Preparation and characterization of lanthanum zirconate. J. Mater. Sci. 33, 4517–4523. https://doi.org/10.1023/A:1004496100596.

Osaka, T., Numako, C., Koto, K., 1999. Local structure and thermal study of ytterbium-doped SrZrO3. Mater. Res. Bull. 34, 11–24. https://doi.org/10.1016/S0025-5408(98)00209-8.

Parida, S., Rout, S.K., Cavalcante, L.S., Sinha, E., Li, M.S., Subramanian, V., Gupta, N., Gupta, V.R., Varela, J.A., Longo, E., 2012. Structural refinement, optical and microwave dielectric properties of BaZrO3. Ceram. Int. 38, 2129–2138. https://doi.org/10.1016/j.ceramint.2011.10.054.

Pfaff, G., 1994. Synthesis of calcium titanate powders by the sol-gel process. Chem. Mater. 6, 58–62. https://doi.org/10.1021/cm00037a013.

Prodromakis, T., Papavassiliou, C., 2009. Engineering the Maxwell-Wagner polarization effect. Appl. Surf. Sci. 255, 6989–6994. https://doi.org/10.1016/j.apsusc.2009.03.030.

Ranjan, R., Vaidya, S., Thaplyal, P., Qamar, M., Ahmed, J., Ganguli, A.K., 2009. Controlling the size, morphology, and aspect ratio of nanostructures using reverse micelles: a case study of copper oxalate monohydrate. Langmuir 25, 6469–6475. https://doi.org/10.1021/la900063q.

Shannon, R.D., 1976. Revised effective ionic radii and systematic studies of interatomic distances in halides and chalcogenides. Acta Crystallogr. Sect. A 32, 751–767. https://doi.org/10.1107/S0567739476001551.

Wang, D., Ye, J., Kako, T., Kimura, T., 2006. Photophysical and photocatalytic properties of SrTiO3 doped with Cr cations on different sites. J. Phys. Chem. B 110, 15824–15830. https://doi.org/10.1021/jp062487p.

Yamaguchi, T., Komatsu, Y., Otobe, T., Murakami, Y., 1980. Newly developed ternary (Ca, Sr, Ba) zirconate ceramic system for microwave resonators. Ferroelectrics 27, 273–276. https://doi.org/10.1080/00150198008226116.

Yamazaki, Y., Hernandez-Sanchez, R., Haile, S.M., 2009. High total proton conductivity in large-grained yttrium-doped barium zirconate. Chem. Mater. 21, 2755–2762. https://doi.org/10.1021/cm900208w.

Yuan, Y., Zhao, Z., Zheng, J., Yang, M., Qiu, L., Li, Z., Zou, Z., 2010. Polymerizable complex synthesis of BaZr1−xSnxO3 photocatalysts: Role of Sn4+ in the band structure and their photocatalytic water splitting activities. J. Mater. Chem. 20, 6772–6779. https://doi.org/10.1039/C0JM00455C.

Yugami, H., Matsuo, S., Ishigame, M., 1995. Persistent spectral hole-burning of Eu3+ and Pr3+ in SrZr1 − xYxO3 crystals. Solid State Ionics 77, 195–200. https://doi.org/10.1016/0167-2738(94)00262-Q.

Zak, A., Feldman, Y., Alperovich, V., Rosentsveig, R., Tenne, R., 2000. Growth mechanism of MoS2 fullerene-like nanoparticles by gas-phase synthesis. J. Am. Chem. Soc. 122, 11108–11116. https://doi.org/10.1021/ja002181a.

Zhang, Y., Liu, M., Wang, J., Shimada, T., Kitamura, T., 2014. Strain tunable ferroelectric and dielectric properties of BaZrO3. J. Appl. Phys. 115,. https://doi.org/10.1063/1.4883298 224107.

Zhao, G., Conder, K., Keller, H., Müller, K.A., 1996. Giant oxygen isotope shift in the magnetoresistive perovskite La1–xCaxMnO3+y. Nature 381, 676–678. https://doi.org/10.1038/381676a0.